

From Far and Near: Perceptual Evaluation of Crowd Representations Across Levels of Detail

Xiaohan Sun
Trinity College Dublin
Ireland
sunx4@tcd.ie

Carol O’Sullivan
Trinity College Dublin
Ireland
Carol.O’Sullivan@tcd.ie

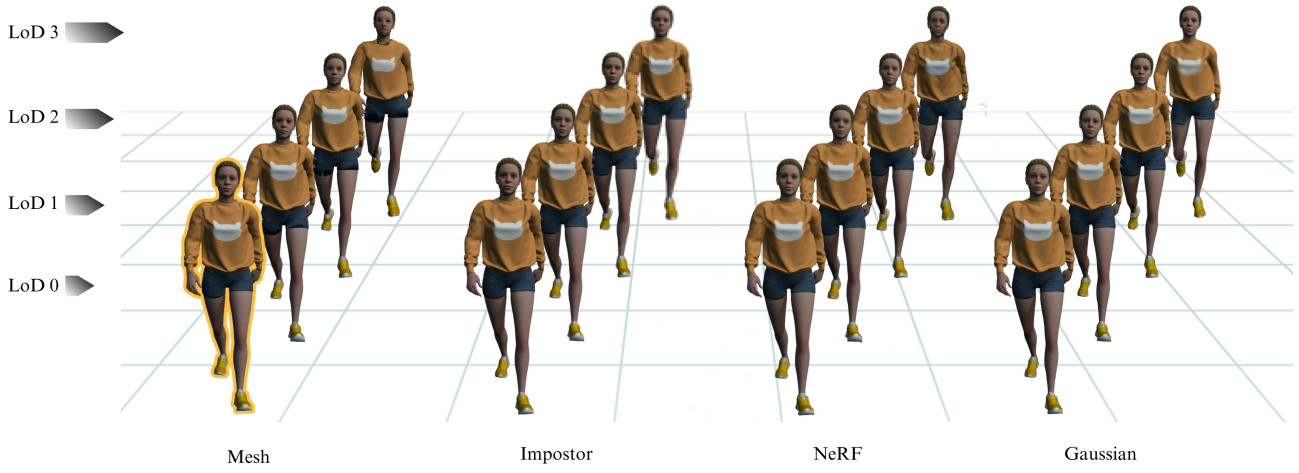


Figure 1. Comparison of four crowd rendering representations (geometric meshes, image-based impostors, Neural Radiance Fields, and 3D Gaussians) across four levels of detail (LoD 0-3). LoD 0 corresponds to the highest resolution (100 %), with detail halved at each subsequent level (50 %, 25 %, 12.5 %). The examples illustrate how fidelity, structural clarity, and smoothness degrade under simplification, revealing characteristic differences among representation types.

Abstract

In this paper, we investigate how users perceive the visual quality of crowd character representations at different levels of detail (LoD) and viewing distances. Each representation—geometric meshes, image-based impostors, Neural Radiance Fields (NeRFs), and 3D Gaussians—exhibits distinct trade-offs between visual fidelity and computational performance. Our qualitative and quantitative results provide insights to guide the design of perceptually optimized LoD strategies for crowd rendering.

Keywords: Crowd rendering, Levels of Detail (LoD), Neural Rendering, Impostor, Perception

1. Introduction

Level of detail (LoD) techniques are widely used in crowd rendering to balance visual realism with performance

efficiency. Simplified geometric meshes and image-based impostors have previously been employed to render large, animated crowds in real time (e.g., [10]). With the recent emergence of neural rendering methods, such as Neural Radiance Fields (NeRF) and 3D Gaussian Splatting (3DGS), a new question is raised: how do traditional LoD approaches compare with modern neural representations; and under what conditions might a neural representation be perceptually equivalent to a high quality mesh representation?

To answer this question, we compare the perceptual impact of LoD rendering for both traditional and neural crowd character representations. Through a controlled user study, we examine which LoD representations are perceptually indistinguishable from a high-resolution, ground-truth mesh at different viewing distances and levels of detail. Our contributions include:

1. **Perceptual thresholds for LoD placement:** We analyze the proportion of times each of the four representations—*Mesh*, *Impostor*, *NeRF*, and *3D Gaussian*—is

judged as most similar to a high-quality mesh. Each representation is evaluated at multiple LoDs and viewing distances, both with and without motion. The resulting perceptual data can inform threshold selection for LoD placement and switching.

2. **Perception-driven LoD pipeline and toolkit.** We introduce a representation-aware LoD rendering pipeline that integrates the four crowd character representations. For reproducibility, we also provide practical guidelines and tools for generating customized LoD assets.

2. Related Work

2.1. Data Representations for Crowd Rendering

Real-time crowd systems have traditionally relied on rigged, skinned *meshes*. In production, assets often share a common rig and topology with per-agent variation in materials and animation clips; engines pack textures into atlases, reuse animation via clip sampling and blending, and issue large instanced draw calls with palette skinning to keep submission overhead low at scale [3, 16].

Image-based approaches replace geometry with 2D view samples, thereby decoupling per-agent cost from polygon count. Early city-scale systems involved the precomputation of atlases over azimuth and animation phases [19]. Later, silhouette errors and texture distortions were reduced by using 2D polygonal proxies [7], or by animating limb impostors independently [2]. A recent neural rendering approach compresses appearance and motion with a CNN to enable constant-time, view-flexible character rendering with explicit material/lighting control [13].

Point-based rendering methods trade connected mesh polygons for point and particle primitives, and can deliver simple, prefilterable samples that are suitable for animation. Early works established the use of points as rendering primitives [9] and introduced surface splatting with anisotropic filters [29]. For animated content, Wand et al. [21] achieved real-time rendering of complex, moving geometry by building multi-resolution hierarchies of prefiltered point sets for keyframed scenes. Ellipsoidal splat formulations extend this idea by using anisotropic kernels with visibility-aware rasterization [29]. This precursor to the ellipsoidal kernels used in modern Gaussian splatting [8] is conceptually akin to point-based rendering, but with learned or optimized appearance parameters.

Neural scene representations provide promising new LoD options beyond polygons and image-based imposters. For example, Neural Radiance Fields (NeRF) can model volumetric radiance via a per-ray multilayer perceptron (MLP) [11]. These are typically converted to explicit or factorized structures for speedy deployment [25, 12]. Gaussian splatting can also deliver real-time rendering using anisotropic splats and a fast, visibility-aware renderer [8],

while space–time extensions tackle dynamic scenes and temporal coherence [24].

2.2. Level of Detail (LoD) for Animated Crowds

LoD rendering for animated crowds may be framed as the process of choosing the least costly representation per character that is perceptually adequate for given viewing conditions. LoD strategies that consider geometry, motion, materials, and behavior have been proposed, incorporating hierarchical reductions of skeletons, meshes, and animation samples to deliver interactive rates at scale. These approaches exploit batching and instancing, GPU-centric skinning and shading, animation compression, and visibility/overdraw control [14, 20, 3, 16].

At larger viewing distances, image-based impostors can be displayed based on the camera viewpoint and each character’s animation pose, thus reducing the overall rendering cost [19]. The viable viewing distance can be further extended by preserving silhouettes using 2D polygonal proxies [7], while per-joint impostors provide more flexibility for varied animations [2]. Point/particle proxies (and displaced-subdivision variants) have also been proposed and compared with image-based methods [15]. Hybrid 2.5D systems, such as *Geopostors* [4], strive to balance memory, draw calls, and temporal plausibility. Viewing distance bands are defined, beyond which geometry is replaced by impostors, and restored when the camera approaches. More recently, neural rendering methods for LoD control have been explored, e.g., by converting NeRF to explicit or factorized forms for faster evaluation, or via native, adaptive detail selection in Gaussian avatars and crowd pipelines [6, 17].

Comparative studies have been conducted to examine the relative advantages of different LoD crowd character representations. McDonnell et al. [10] systematically compared image-based impostors with low-resolution geometric meshes, with respect to appearance and motion fidelity. More recently, Sun et al. [18] examined the perceived quality of 3D Gaussian avatars based on motion, level of detail, and distance. In this paper, we extend this body of work by comparing the perceived quality of *Mesh*, *Impostor*, *NeRF*, and *3D Gaussian* representations of animated characters across different LoDs and viewing distances.

3. Implementation Methods

3.1. Mesh

Our gold-standard representation is a high-resolution mesh of a female character walking for 60 frames, downloaded from Mixamo. [1] Each frame is also captured from 60 cameras on a hemispherical rig (3,600 images in total; see Figure 2).

Our four Mesh LoDs are generated using Blender’s Dec-



Figure 2. Examples of data.

imate modifier. The base model (L0) and three simplified versions are created by applying decimation ratios of 1.0, 0.5, 0.25, and 0.125, yielding face counts of 27,048; 18,436; 10,811; and 5,864 respectively. Reducing the polygon count of animated characters to generate geometric mesh LoDs is a common practice to improve rendering performance in crowds [3, 5]. Edge-collapse or “collapse” type decimation (as used in Blender) provides control over face count reduction while preserving shape and animation fidelity.

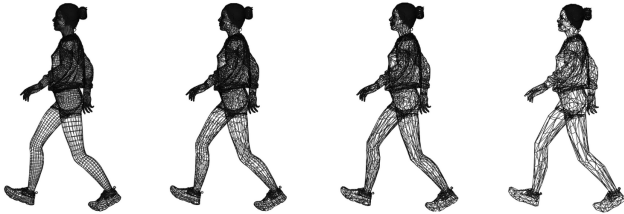


Figure 3. Examples of mesh LoD.

3.2. Impostor

For our second representation, the animated character is rendered as a precomputed impostor sequence packed into a 6×10 sprite sheet per LoD. At the highest level (L0), each tile consists of 1080×1080 pixels, which matches the resolution used to render the reference mesh. Each lower level halves the resolution to 540×540 , 270×270 , and 135×135 px (L1–L3). To avoid the per-frame “breathing” and root-motion loss typical of naive per-frame crops, we first compute a *union* alpha bounding box over all frames of the run cycle, crop every frame to that fixed window, and apply a single global scale per LoD before centering on a square canvas. The stabilized frames are then packed column-major into a texture atlas that Blender reads as a single image. At render time we use an unlit material and animate UVs over a sprite-sheet atlas: the UVs are cropped to a single tile and offset at each frame so that the impostor displays one precomputed pose at a time. This workflow follows standard impostor practice, replacing distant geometry by a textured quad while indexing an atlas of animation frames. It is widely used in crowd rendering for

performance, with quality governed by atlas resolution and sampling order [19]. To match the baked appearance, we fix the impostor’s pose and world position to the capture setup and render from the same camera transform and FOV used during capture.

3.3. NeRF

We implement NeRF as our third representation, using *Instant-NGP*, which replaces the original fully connected NeRF with a multiresolution hash-grid encoding feeding a compact MLP, substantially reducing training and inference cost while retaining quality [11, 12]. LoD is controlled via the hash table capacity and network width: we fix the number of hash levels L and features per level F , and from L0 to L3 successively halve the hash capacity (decreasing $\log_2 T$ by 1 per step) while modestly narrowing the MLP. Exact presets appear in Table 1. For animation, we reconstruct independent NeRFs for each of 60 frames and render them from a shared camera path, yielding a frame-wise dynamic sequence. To validate that L0 serves as a suitable upper bound, we evaluated it on 60 held-out views, obtaining PSNR = 36.18 and SSIM = 0.988, indicating high-fidelity reconstruction.

3.4. Gaussian Splatting

3D Gaussian Splatting is our fourth representation, with a visibility-aware rasterizer and anisotropic splats [8]. Fidelity is controlled by *capping the Gaussian count N* . For large reductions we apply a light opacity prune ($\alpha < 0.01$). Our four presets are $N=\{120k, 30k, 7.5k, 1.9k\}$ for L0 to L3, resp. All LoDs use the same optimization recipe: an L_1 +SSIM loss, spherical-harmonic color basis of degree 2, and Adam optimizer. Each continuation runs for 20k steps. LoD is applied with a simple count budget and a light opacity prune. This practical setup is compatible with recent approaches that address aliasing via scale-aware filtering and reduce model size through learned pruning [26, 28]. As with NeRF, we optimize a separate 3DGS per frame for 60 frames and render from a common camera, producing the dynamic sequence. L0 achieves PSNR = 36.69 and SSIM = 0.991 on 60 held-out views, confirming that our highest-detail preset provides a strong reference for comparisons.

4. Experimental Design

4.1. User Study

Stimuli. Four representations were displayed: Image-based Impostors (**I**), Meshes (**M**), NeRFs (**N**), and 3D Gaussians (**G**). Four levels of detail were created: (L0=100%, L1=50%, L2=25%, L3=12.5%) and five viewing distances (D0=100% pixels, D1=80%, D2=60%, D3=40%, D4=20%). In each trial, the four representations were displayed side by side in counterbalanced order. Participants

Table 1. Instant-NGP LoD presets. L : hash levels; F : features/level; $T = 2^{\log_2 \text{hashmap.size}}$.

LoD	L	F	$\log_2 T$	Base res.	Density MLP (neurons, layers)	Dir. enc.	RGB net (neurons, layers)
LoD-0	12	2	18	16	128, 1 \times	SH deg. 4 + Identity	64, 2 \times
LoD-1	12	2	17	16	64, 1 \times	SH deg. 3 + Identity	32, 2 \times
LoD-2	12	2	16	16	32, 1 \times	SH deg. 2 + Identity	16, 2 \times
LoD-3	12	2	15	16	16, 1 \times	SH deg. 1 + Identity	16, 1 \times

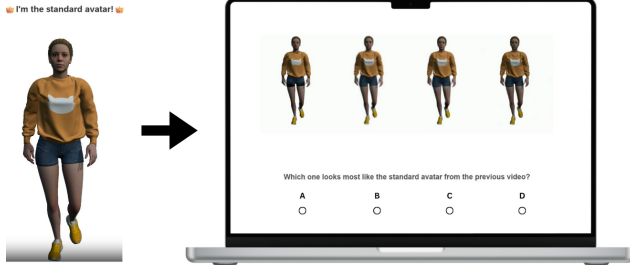


Figure 4. Example of video stimulus.

completed two blocks: a) *Video* (with motion) and *Image* (with no motion).

Participants and procedure. Twenty-four volunteers (17 male, 7 female; age 18–60+) completed a brief training session followed by two trial blocks (Video and Image). The experiment was conducted online via Qualtrics and was fully anonymous. For each trial, participants viewed a high-resolution mesh reference and then chose with one of the four displayed stimuli most closely matched the high-quality mesh (see Fig. 4). Trials were randomized, and the positions of the four representations were counterbalanced across participants.

Statistical analysis. Choices were analyzed as fully within-subjects repeated measures with factors *Representation* (G, I, M, N), *Distance* (D0–D4), and *LoD* (L0–L3), in both *Modes* (Image vs. Video). We averaged the repetitions per participant and condition to obtain selection proportions. We fitted an OLS with subject fixed effects and the full *Representation* \times *Distance* \times *LoD* \times *Mode* factorial, and report a Type II ANOVA (Table 2). Because responses are binary at the trial level, we additionally fitted a trial-level binomial GLM (logit) with subject fixed effects, and obtained likelihood-ratio omnibus tests by comparing the full model to hierarchically reduced models (Table 3). Descriptive means (\pm SE) are shown in Figs. 5.

Results. The ANOVA revealed a strong main effect of *Representation*, as well as robust *Representation* \times *Distance* and *Representation* \times *LoD* interactions. The three-way interaction *Representation* \times *Distance* \times *LoD* was also significant. No main effects of *Distance*, *LoD* or *Mode* (Image vs. Video) were observed and no interactions involving *Mode* reached significance (min $p = 0.257$). The confirmatory trial-level GLM echoed these patterns with significant omnibus LR tests for *Representation*, *Distance*, *LoD*, *Repre-*

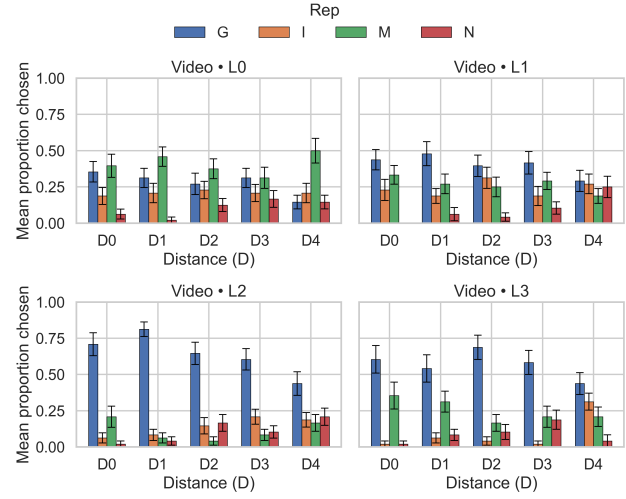


Figure 5. Video block: mean proportion chosen for each representation across LoD and Distance (D0–D4). Error bars show ± 1 SE across participants.

sentation \times *LoD*, *LoD* \times *Distance*, and the three-way interaction (Table 3).

Discussion. Perceived fidelity is seen to depend on a combination of *Representation*, viewing *Distance*, and *LoD*. As expected, **Mesh** is most preferred at high detail and near distances, whereas **Gaussians** become increasingly indistinguishable from the Mesh as detail decreases and/or viewing distance increases. Both the omnibus ANOVA and the confirmatory GLM reveal strong effects of *Representation*, clear interactions with *LoD*, and a significant three-way interaction, whereas no significant main or interaction effect was found for *Mode* (Image vs. Video).

4.2. Quantitative Experiments

4.2.1 Visual Comparison

Image fidelity is calculated using an evaluation view camera that combines poses matching the user-study setup but is excluded from NeRF/3DGS training. For each LoD and representation, we compare with the Mesh reference in the same pose using PSNR, SSIM and LPIPS [23, 22, 27]. Table 4 reports metrics across LoDs; higher PSNR/SSIM and lower LPIPS indicate closer agreement with the Mesh baseline.

Table 2. ANOVA showing the results of main and interaction effect tests with degrees of freedom, effect sizes (η^2) and (p) values. (Common denominator df for the OLS Type II ANOVA is 3657.)

Effect Tested	dof	F-Test	η^2	p
Representation	3	177.52	0.127	< 0.001
Representation \times Distance	12	8.53	0.027	< 0.001
Representation \times LoD	9	33.16	0.075	< 0.001
Representation \times Mode	3	1.08	0.001	0.356
Representation \times Distance \times LoD	36	2.26	0.022	< 0.001
Representation \times Distance \times Mode	12	0.36	0.001	0.976
Representation \times LoD \times Mode	9	0.90	0.002	0.527
Representation \times Distance \times LoD \times Mode	36	1.14	0.011	0.257

Table 3. Omnibus likelihood-ratio (LR) tests from the trial-level binomial GLM with subject fixed effects.

Effect	LR	df	p
Representation	1089.30	139	< 0.001
Distance	275.81	140	< 0.001
LoD	418.92	136	< 0.001
Mode	66.02	80	0.869
Representation \times Distance	61.83	76	0.880
Representation \times LoD	418.92	121	< 0.001
Representation \times Mode	66.02	79	0.851
LoD \times Distance	152.80	124	0.040
Representation \times LoD \times Distance	150.97	112	0.008

Summary. At L0, both **3D Gaussians** and **NeRF** closely match the Mesh (Gaussians: 36.69 dB / 0.991 / 0.013; NeRF: 36.18 dB / 0.988 / 0.019 for PSNR / SSIM / LPIPS). With decreasing LoD, **NeRF** degrades smoothly in PSNR while maintaining high SSIM and low LPIPS; **Gaussians** show a larger PSNR drop but remain competitive on SSIM/LPIPS through mid LoDs. **Impostors** exhibit high SSIM and very low LPIPS at the matched view, despite lower PSNR, consistent with view-aligned textures that preserve structure but lack 3D parallax. Overall, frame-based metrics indicate that neural fields (NeRF/3DGS) are closest to Mesh at high detail, while impostors can appear perceptually similar at single views even with lower pixel-wise fidelity.

4.2.2 Memory Usage

We quantify deployment memory as the on-disk size of the exact LoD assets used in the study. This metric is engine-agnostic and comparable across heterogeneous toolchains. Table 5 reports the footprint per representation and LoD. The entries correspond to (i) **Mesh**: the rigged mesh package (geometry; armature; textures), (ii) **Impostor**: billboard atlas images (iii) **3D Gaussian**: the optimized Gaussian caches, and (iv) **NeRF**: model snapshots.

Table 4. Image Similarity at Evaluation View.

Rep.	LoD	PSNR \uparrow	SSIM \uparrow	LPIPS \downarrow
NeRF	L0	36.18	0.988	0.019
	L1	35.08	0.984	0.022
	L2	33.25	0.977	0.030
	L3	28.09	0.954	0.052
3DGS	L0	36.69	0.991	0.013
	L1	24.76	0.961	0.029
	L2	24.52	0.954	0.045
	L3	24.01	0.938	0.090
Impostor	L0	23.95	0.965	0.006
	L1	23.40	0.970	0.010
	L2	21.35	0.970	0.017
	L3	19.40	0.971	0.030

Table 5. On-disk asset size by representation and LoD (as used in the study).

Representation	LoD0	LoD1	LoD2	LoD3
NeRF	21.2 MB	17.0 MB	15.5 MB	14.0 MB
3D Gaussian	19.0 MB	8.00 MB	2.00 MB	0.768 MB
Impostor	328 KB	100 KB	32.0 KB	12.0 KB
Mesh	5.19 MB	4.37 MB	3.86 MB	3.50 MB

Summary. Deployment footprint varies significantly by representation. **Impostors** are the most memory-efficient by a wide margin and scale down aggressively with decreasing LoD. **3D Gaussians** also exhibit strong compressibility, offering a tunable 3D option that needs less memory than Mesh with decreasing LoDs. In contrast, **Mesh** assets yield only modest savings with simplification, reflecting limits imposed by geometry and rig data, while **NeRFs** require the most memory resources across LoDs with comparatively smaller proportional reductions.

5. Conclusions and Future Work

Our results show that perceived similarity to a mesh ground truth is driven primarily by a character’s *Representation* and its interactions with *Distance* and *LoD*, and does not appear to be affected by the presence or absence of mo-

tion.

Based on these results, we propose the following practical guidelines: **Impostors** are the cheapest and most scalable choice for far/low-detail rendering (i.e., minimal geometry cost and excellent batching at distance), although flexibility is sacrificed for large precomputed atlases and limited animation blending. **3D Gaussians** become increasingly indistinguishable from meshes as pixel density drops or detail is reduced, thus offering a strong mid-to-high LoD alternative with real-time rendering. Geometric **Meshes** retain a clear advantage at nearer views and higher detail, but for further distances, more efficient representations are highly competitive. Table 6 summarizes authoring considerations, and Table 7 lists data-prep and per-frame optimization times for our LoD presets.

Behavioural fidelity beyond appearance: Our study explores visual fidelity only, whereas convincing *motion and behaviour* is also important for practical applications. Future evaluations could couple perceptual factors with behavioral realism (e.g., locomotion quality, local interactions, group coherence) so that LoD scheduling decisions reflect both what is seen and how agents move.

Adaptive LoD switching: Rather than using pre-defined settings, a natural next step would be an automatic LoD scheduling policy that updates in real time as the user moves and the scene context changes. Such a controller could be tuned or learned from user data and plugged into a hybrid stack to ensure high quality while meeting performance targets.

In summary, we present a unified perceptual framework spanning Mesh, Impostor, NeRF, and 3D Gaussian representations, and provide guidelines on managing LoD displays for crowd systems. We also describe a practical LoD pipeline and toolkit for generating customizable crowd assets based on these four representations, thereby enabling artists to select and combine methods to meet fidelity and performance targets.

Table 6. Authoring & integration rubric. Scores: +++ = strong, ++ = moderate, + = limited, - = poor, — = none.

Representation	Tooling	Automation	Motion flexibility	Appearance flexibility	Physics
Mesh	+++	+	+++	+++	+++
Impostor	++	+++	-	-	-
NeRF	-	++	+	-	-
Gaussian	-	++	++	-	-

Interpretation. *Tooling* = maturity of engine support and libraries. *Automation* = batchability in our scripts. *Motion flexibility* = ability to swap in novel motions. *Appearance flexibility* = assets editability. *Physics* = compatibility with modern physics pipelines.

Table 7. Preprocessing and per-frame optimization times in our implementation pipeline.

Representation	Data prep	Offline training (s)
Mesh	60 cameras \times 60 frames render capture; export LoDs via Blender <i>Decimate</i>	—
Impostor	Union-alpha bbox stabilization; pack 6 \times 10 sprite sheets per LOD	—
NeRF (Instant-NGP [12])	Camera intrinsics & poses from COLMAP; graphics-convention export (x right, y up, -z)	L0: \sim 240 L1: \sim 207 L2: \sim 214 L3: \sim 205
3D Gaussian (3DGS [8])	Camera intrinsics & poses from COLMAP; sparse colored SfM to initialize splats	L0: \sim 320 L1: \sim 122 L2: \sim 78 L3: \sim 58

Interpretation. *Data prep* covers all the steps involved prior to the rendering of representations. *Offline training* reports per-frame optimization at **20k** steps for each LoD preset, running on an RTX4090.

Acknowledgement

This work was conducted with the financial support of the Research Ireland Centre for Research Training in Digitally-Enhanced Reality (d-real) under Grant No. 18/CRT/6224. For the purpose of Open Access, the author has applied a CC BY public copyright licence to any Author Accepted Manuscript version arising from this submission.

References

[1] Adobe. Mixamo. <https://www.mixamo.com/>. Accessed 2025-10-13. 2

[2] Á. Beacco, N. Pelechano, and C. Andújar. Efficient rendering of animated characters through optimized per-joint impostors. *Computer Animation and Virtual Worlds*, 23(3-4):331–339, 2012. 2

[3] A. Beacco, N. Pelechano, and C. Andújar. A survey of real-time crowd rendering. *Computer Graphics Forum*, 35(8):32–50, 2016. 2, 3

[4] S. Dobbyn, J. Hamill, K. O’Conor, and C. O’Sullivan. Geopostors: A real-time geometry/impostor crowd rendering system. In *Proceedings of the Symposium on Interactive 3D Graphics and Games (I3D)*, pages 95–102, 2005. 2

[5] Y. Dong and C. Peng. Real-time large crowd rendering with efficient character and instance management on gpu. *International Journal of Computer Games Technology*, 2019(1):1792304, 2019. 3

[6] X. Dongye, H. Guo, L. Luo, H. Jiang, Y. Bao, Z. Tian, and D. Weng. Lodavatar: Hierarchical embedding and adaptive levels of detail with gaussian splatting for enhanced human avatars. arXiv:2410.20789, 2024. 2

[7] L. Kavan, S. Dobbyn, S. Collins, J. Žára, and C. O’Sullivan. Polypostors: 2d polygonal impostors for 3d crowds. In *Proceedings of the Symposium on Interactive 3D Graphics and Games (I3D)*, pages 149–155, 2008. 2

[8] B. Kerbl, G. Kopanas, T. Leimkühler, and G. Drettakis. 3d gaussian splatting for real-time radiance field rendering. *ACM Transactions on Graphics*, 42(4):1–14, 2023. 2, 3, 7

[9] M. Levoy and T. Whitted. The use of points as a display primitive. Technical Report TR 85-022, Department of Computer Science, University of North Carolina at Chapel Hill, 1985. 2

[10] R. McDonnell, S. Dobbyn, and C. O’Sullivan. Lod human representations: A comparative study. In *V-CROWDS: Intl. Workshop on Crowd Simulation*, pages 101–115, 2005. 1, 2

[11] B. Mildenhall, P. P. Srinivasan, M. Tancik, J. T. Barron, R. Ramamoorthi, and R. Ng. Nerf: Representing scenes as neural radiance fields for view synthesis. In *ECCV*, 2020. 2, 3

[12] T. Müller, A. Evans, C. Schied, and A. Keller. Instant neural graphics primitives with a multiresolution hash encoding. *ACM Transactions on Graphics (SIGGRAPH)*, 41(4):1–15, 2022. 2, 3, 7

[13] M. Ostrek, N. J. Mitra, and C. O’Sullivan. Neuropostors: Neural geometry-aware 3d crowd character impostors. In *Pattern Recognition: 27th International Conference, ICPR 2024, Kolkata, India, December 1–5, 2024, Proceedings, Part XXII*, volume 15322 of *Lecture Notes in Computer Science*, pages 432–448. Springer, 2024. 2

[14] C. O’Sullivan, J. Cassell, J. Dingliana, S. Dobbyn, B. McNamee, C. Peters, and T. Giang. Levels of detail for crowds and groups. *Computer Graphics Forum*, 21(4):733–741, 2002. 2

[15] I. Rudomín and E. Millán. Point-based rendering and displaced subdivision for interactive animation of crowds of clothed characters. In *VRIPHYS 2004: Virtual Reality Interaction and Physical Simulation Workshop*, pages 139–148, 2004. 2

[16] G. Ryder, M. Chalmers, and R. McCready. A survey of real-time rendering techniques for crowds. In *Eurographics State of the Art Reports*. 2005. 2

[17] X. Sun, Y. Xu, J. Dingliana, and C. O’Sullivan. Crowd-splat: Exploring gaussian splatting for crowd rendering. arXiv:2501.17792, 2025. Includes LoD integration for crowd-scale rendering. 2

[18] X. Sun, Y. Xu, J. Dingliana, and C. O’Sullivan. Evaluating crowd-splat: Perceived level of detail for gaussian crowds. In *2025 IEEE Conference on Virtual Reality and 3D User Interfaces Abstracts and Workshops (VRW)*, pages 720–724. IEEE, 2025. 2

[19] F. Tecchia, C. Loscos, and Y. Chrysanthou. Image-based crowd rendering. *IEEE Computer Graphics and Applications*, 22(2):36–43, 2002. 2, 3

[20] L. Toledo, O. D. Gyves, and V. Rudomín. Hierarchical level of detail for varied animated crowds. *The Visual Computer*, 30(6):949–961, 2014. 2

[21] M. Wand and W. Straßer. Multi-resolution rendering of complex animated scenes. *Computer Graphics Forum*, 21(3):483–491, 2002. Proc. Eurographics 2002. 2

[22] Z. Wang, A. C. Bovik, H. R. Sheikh, and E. P. Simoncelli. Image quality assessment: From error visibility to structural similarity. *IEEE Transactions on Image Processing*, 13(4):600–612, 2004. 4

[23] S. Wolf and M. Pinson. Reference algorithm for computing peak signal-to-noise ratio (psnr) of a video sequence with a constant delay. Contribution com 9–c 6, ITU-T Study Group 9 (contribution from NTIA/ITS, USA), Geneva, Switzerland, Feb. 2009. Defines a standardized PSNR computation procedure for video. 4

[24] G. Wu, T. Yi, J. Fang, L. Xie, X. Zhang, W. Wei, W. Liu, Q. Tian, and X. Wang. 4d gaussian splatting for real-time dynamic scene rendering. In *CVPR*, 2024. 2

[25] A. Yu, R. Li, M. Tancik, L. Hao, R. Ng, and A. Kanazawa. Plenoctrees for real-time rendering of neural radiance fields. In *ICCV*, 2021. 2

[26] Z. Yu, B. Kerbl, C. Xie, N. Rüegg, S. I. Liu, and A. Geiger. Mip-splatting: Alias-free 3d gaussian splatting. In *CVPR*, 2024. 3

[27] R. Zhang, P. Isola, A. A. Efros, E. Shechtman, and O. Wang. The unreasonable effectiveness of deep features as a perceptual metric. In *Proceedings of the IEEE/CVF Conference on Computer Vision and Pattern Recognition (CVPR)*, pages 586–595, 2018. 4

- [28] Z. Zhang, T. Song, Y. Lee, L. Yang, C. Peng, R. Chellappa, and D. Fan. Lp-3dgs: Learning to prune 3d gaussian splatting. In *NeurIPS*, 2024. 3
- [29] M. Zwicker, H. Pfister, J. van Baar, and M. Gross. Surface splatting. In *Proceedings of the 28th Annual Conference on Computer Graphics and Interactive Techniques (SIGGRAPH '01)*, pages 371–378. ACM, 2001. 2